A Distinct Molecular Mechanism by which Phenytoin Rescues a Novel Long QT 3 Variant. Ivan Gando, Chiara Campana, Reina Bianca Tan, Frank Cecchin, Eric A. Sobie, William A. Coetzee

EXPANDED METHODS AND RESULTS

Cell Culture

Human embryonic kidney 293 (HEK-293) cells were cultured in Dulbecco's Modified Eagle Media (Thermo Fisher Scientific, Waltham, MA) with heat-inactivated 10% fetal bovine serum and penicillin-streptomycin. Wild-type (WT) or mutant $Na_v1.5$ cDNAs (0.9 µg), together with an EGFP plasmid (0.1 µg), were transiently co-transfected using Lipofectamine 2000 (Life Technologies, Carlsbad, CA).

Biotinylation assays

Cells were washed with Dulbecco's phosphate-buffered saline and biotinylated for 30 min using phosphate-buffered saline (PBS) containing 0.5 mg/mL of EZ Link Sulfo-NHS-SS-Biotin (Thermo Fisher Scientific). Excess biotin was quench with 100 mM glycine and cells were lysed with RIPA buffer (Sigma Aldrich, St. Louis, MO, USA). After centrifugation at 14,000 × *g* for 15 min, supernatants were incubated overnight with NeutrAvidin beads (Pierce, Appleton, WI) and pelleted by centrifugation 1,000 × *g* for 1 min. All steps were performed at 4°C. The biotinylated proteins were eluted with the Laemmli sample buffer (Bio-Rad Laboratories, Hercules, CA, USA) with 50 mM DTT at room temperature for 1 h and analyzed by Western blotting.

Western blotting

Protein concentration was measured using a protein assay dye reagent (Bio-Rad Laboratories). Equal amounts of total protein were mixed with sample buffer (Thermo Fisher Scientific) containing 50 mM DTT and kept at room temperature prior to resolving with a 4–15% polyacrylamide gradient gel. After transfer to polyvinylidene difluoride membranes (Bio-Rad) and blocking with 5% milk in TBS-Tween (0.05%) for 1 h, blots were incubated overnight at 4°C with primary antibodies and 1 h at room temperature with secondary antibodies (dissolved in blocking buffer). Detection was with chemiluminesence (SuperSignal West Dura, Thermo Fisher Scientific). Immunoblots were analyzed and quantified using ImageJ [10].

Patch Clamping

Whole-cell $Na_v1.5$ currents were recorded 48 h after transfection using patch clamp techniques at 22–24°C (Axopatch 200B; Molecular Devices, Sunnyvale, CA). Currents were low-pass filtered

with 8-pole Bessel filter (-3dB @ 1 Hz) and digitized at 3 kHz (DigiData 1550A, Molecular Devices) using pClamp v10.5 software. Patch electrodes were manufactured (Zeitz, Germany) using borosilicate glass (1.5 mm OD; World Precision Instruments, Sarasota, FL) and had tip resistances of 2-3 MΩ when filled with (in mmol/L): 10 KCl, 105 CsF, 10 NaCl, 10 HEPES, 10 EGTA, and 10 TEA-Cl and pH adjusted to 7.2 with 2N CsOH. The bath solution consisted of (in mmol/L): 30 CsCl, 107 NaCl, 5.4 KCl, 10 HEPES, 0.5 $MgCl_2$, 1.8 $CaCl_2$ with pH 7.4 adjusted with 2N NaOH. Data were not corrected for the liquid junction potential, calculated to be 7.4 mV. The whole-cell capacitance and series resistance were compensated to levels greater than 80%. Currents were corrected for cell size by dividing membrane current by the cell capacitance.

Site-directed Mutagenesis

The human $Na_v1.5$ cDNA in pcDNA3.1 (a gift from Nicole Schmitt, Ph.D., University of Copenhagen) was subjected to site-directed mutagenesis (Quickchange II XL, Aligent Technologies, Santa Clara, CA) using primer 5'-GACAACTTCAACCCACAGAAGAAAAAGTTAGGGGC-3' to generate $Na_v1.5$-Q1475P. The cDNAs were verified by sequencing (Macrogen USA, Rockville, MD).

Patch Clamp Data Analysis

Data were plotted using Origin Pro 8 (OriginLab, Northampton, MA). Current-voltage curves were produced by plotting the $Na_v1.5$ peak current density against the clamp step potential. To generate activation curves, peak inward currents (I_{Na}) were converted to conductance as follows: $G_{Na} = I_{Na}/(E_m - E_{rev})$, where E_m is the clamp step voltage and E_{rev} the reversal potential, which was determined for each cell. Values of G_{Na} were normalized to the maximum conductance and plotted as a function of voltage. The voltage dependence of steady-state inactivation was determined using pre-pulse voltage steps from -160 mV to -20 mV (500 ms at 10 mV increments), prior to a clamping at a test voltage of -20 mV. Peak currents during the test step were normalized to the maximum current amplitude. Data points were subjected to curve fitting using a Boltzmann equation, $1/[1 + \exp[(V_m - V_{½})/k]]$, with V_m the pre-pulse potential, $V_{½}$ the midpoint of activation or inactivation, and k the slope factor. The inactivation process was analyzed by curve fitting of decaying currents to $[A_f * \exp(t/\tau_f)] + [A_s * \exp(t/\tau_s)]$, where A is the amplitude of the fit, t the time, τ the time constant. Recovery from inactivation was measured using a standard two-pulse protocol to -20 mV from a holding potential of -120 mV. The voltage between the pulses was -120 mV and was varied between 0.5 to 500 ms. Peak currents during the second step were normalized to those during the first step, plotted against the recovery time and subjected to curve fitting to $A * \exp(t/\tau)]$, with τ the recovery time constant.

Computational approach to $Na_v1.5$ modeling

Simulations that attempted to recapitulate the experimental electrophysiology protocols with the original Markov model led to extremely different results compared to WT channels experiments, partly due to the fact that the model was published for mouse data. We therefore adjusted rate constants in the Markov model to match the experimental data, and used a genetic algorithm for this optimization procedure. An initial random population for the algorithm was generated by scaling each rate constant by a factor between 0.1 and 10 times its original one, with scale factors randomly selected from a log-uniform distribution. The voltage dependence of each rate constant was identical to that in the original published model.

An initial population of size 200 was used for simulating treated and untreated Q1475P channels, while a larger population (n=500) was used for WT channels. This increase in population size together with a larger number of generations allowed the simulations to cover a wider parameter space and reach the same desired fitness for all three groups.

Default MATLAB values were used for the genetic algorithm options. These include the tournament selection size, which is equal to 4, the crossover fraction, which is equal to 0.8, and the mutation function, which was set equal to a gaussian distribution with default scale and shrink values.

At each generation, a fitness score was calculated for each individual of the population as:

$$fitness = \sum_{1}^{n} (y_i - x_i)^2$$

Where, y and x represent the simulated value and the experimental value respectively. The index *i* represents the value of either voltage or inter-pulse interval at which the functions x and y are evaluated. This formula was utilized to individually compute the fitness score for each protocol: steady-state activation, steady-state inactivation, recovery from inactivation. For the three protocols, we respectively summed over 10 voltage values, 13 voltage values, and 23 intervals. The overall fitness value for each individual in the popluation was then obtained by adding the individual scores.

Multiple runs (n=5) of the genetic algorithm identified three subpopulations of channel variants that describe the gating of WT channels, Q1475P channels, and Q1475P channels treated with drug. In acute drug application experiments, phenytoin and mexiletine did not show any significant

difference in their effects on activation, inactivation or recovery from inactivation of Q1475P channels. Therefore, in our $Na_v1.5$ gating simulations we considered Q1475P channels treated with phenytoin and mexiletine as equivalent and describe them in the text as drug treated Q1475P channels.

Action potential simulations

The ventricular human cardiomyocyte model published by O'Hara et al., specifically this model's endocardial variant, was used as baseline model for our action potential simulations. In the model the sodium current is described by a Hodgkin–Huxley formulation**.** We updated the expression of the sodium current in the model by integrating the Markov models of WT, Q1475P, and Q1475P drug treated channels. The rate constant $\beta_{11,}$ that was not significantly different among the three groups, was scaled in all groups by a factor of 5. This modification, consistent across the groups, ensured that the action potential produced by the median $Na_v1.5$ channel in the WT group matched the action potential duration in the original O'Hara model. We studied the difference between treatment with phenytoin and mexiletine by incorporating in the model the effect of the two drugs on sodium current density. Based on the experimental finding that mexiletine but not phenytoin restores the defective trafficking of $Na_v1.5$ channels after 48 hours of treatment, the maximal conductance for Na^+ current (G_{Na}) was equal to 100% of WT for mexiletine treated cardiomyocytes while it was decreased to 50% of WT, the same value as for untreated Q1475P channels, for phenytoin treated cardiomyocytes.

Action potentials were generated at 1.25 Hz (200 stimuli) by current pulses (80 μA/μF for 0.5 ms).

Action potential duration at 90% of repolarization (APD_{90}) and Na^+ current were recorded. Ordinary differential equations were implemented in MATLAB 2016b and solved using the built-in solver ode15s for stiff differential equations.

Action potential clamp simulations

Action potential clamp simulations were performed to investigate how the occupancy of the different states of the $Na_v1.5$ channel varied between WT, Q1475P and Q1475P drug treated channels throughout the course of an action potential. A standard action potential trace of 200 stimuli was generated running the original O'Hara model at 1Hz. This trace was fed as input to the models of the three groups of channels so that we could study the effect of the different rate constants on the state occupancy. We analyzed the median behavior of the three channels

immediately preceding the last action potential in the sequence, corresponding to diastole at steady-state 1 Hz pacing. The nine states of the $Na_v1.5$ Markov model were grouped into closed (C_3, C_2 and C_1) states, inactivated closed (IC_3, IC_2, IF) states and deep inactivated (I_1, I_2) states. The probability with which WT, Q1475P and Q1475P drug treated channels occupied these three groups of states in diastole was analyzed.

Simulations of heterozygote Q1475P cells

The simulations presented in Figure 8 were of homozygotic Q1475P cells in that all $Na_v1.5$ channels in each cell were assumed to exhibit gating modifications characteristic of the mutation. More precisely, in for the Q1475P action potential shown in Figure 8A, Na^+ channels were described by the nine state Markov scheme with transition rates equal to the median of the five parameter sets identified by the genetic algorithm to describe Q1475P channel gating properties. We also simulated the heterozygotic condition by performing simulations in which 50% of $Na_v1.5$ channels exhibited WT properties and 50% exhibited Q1475P gating. Specifically, heterozygote $Na_v1.5$ channels were described by a Markov model with eighteen states, two sets of the same states. Transitions in one set of states are regulated by median Q1475P transition rates, while transitions in the other nine states are regulated by median WT transition rates. This is to represent that roughly 50% of channels in the cell has normal gating properties while the other half is altered by the Q1475P mutation. The total I_{Na} current is a result of the weighted average of the current flowing through the “WT open state” and the “Q1475P open state”. The value of maximal conductance used to compute the current carried by the Q1475P channels was equal to 50% of the WT G_{Na}. Figure S2 shows the results obtained when the two Markov models are integrated into the ventricular cardiac myocyte model to describe action potentials of heterozygous and homozygous cells. Action potentials were generated at 1 Hz (200 stimuli) by current pulses (80 μA/μF for 0.5 ms).

SUPPLEMENTAL FIGURES

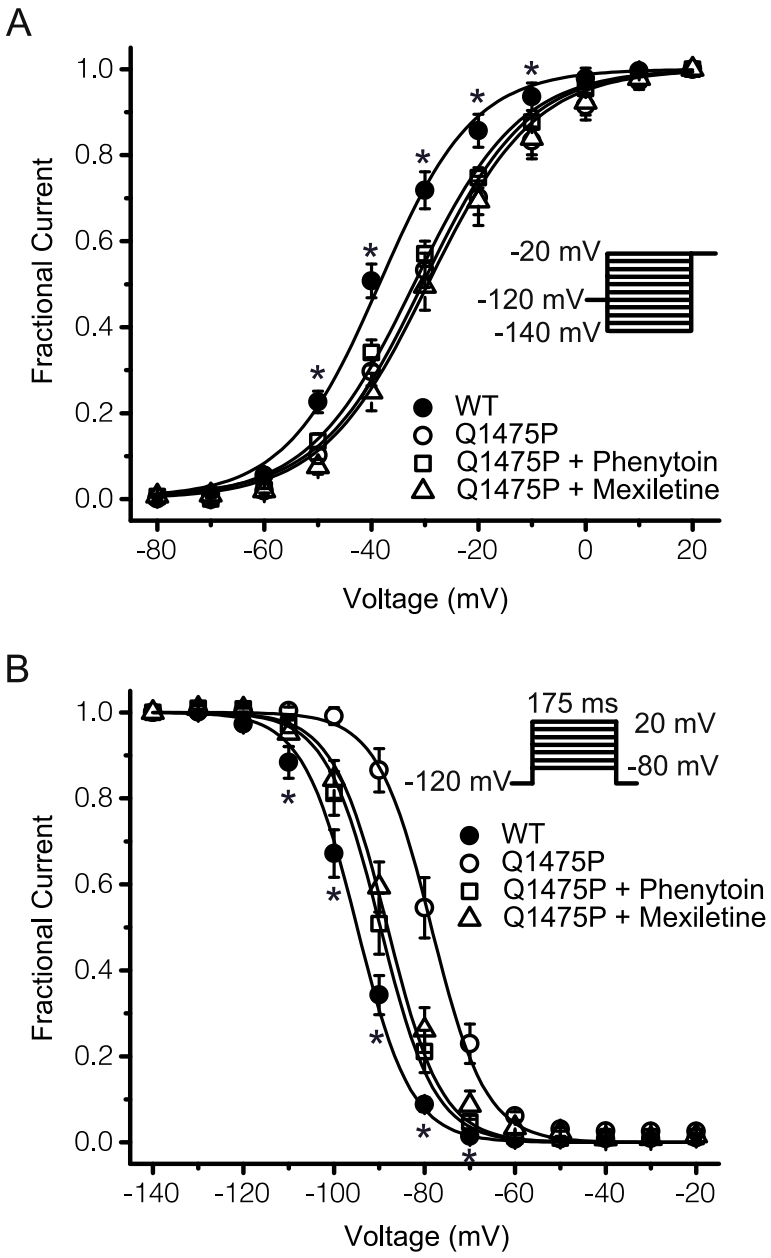

Figure S1: Mexiletine and phenytoin partially restore channel steady-state properties. Steady-state activation (A) and inactivation (B) curves for WT (n=18); Q1475P (n=16); Q1475P + phenytoin (n=13) and Q1475P + mexiletine (n=7). Data points were subjected to curve fitting to a Boltzmann function and the solid lines were derived from the averaged fitted parameters. Phenytoin and mexiletine were each applied at 100 μM. Effects of the drug was compared to WT using a 1W-ANOVA, followed by a Dunnet's t-test. *$p<0.05$.

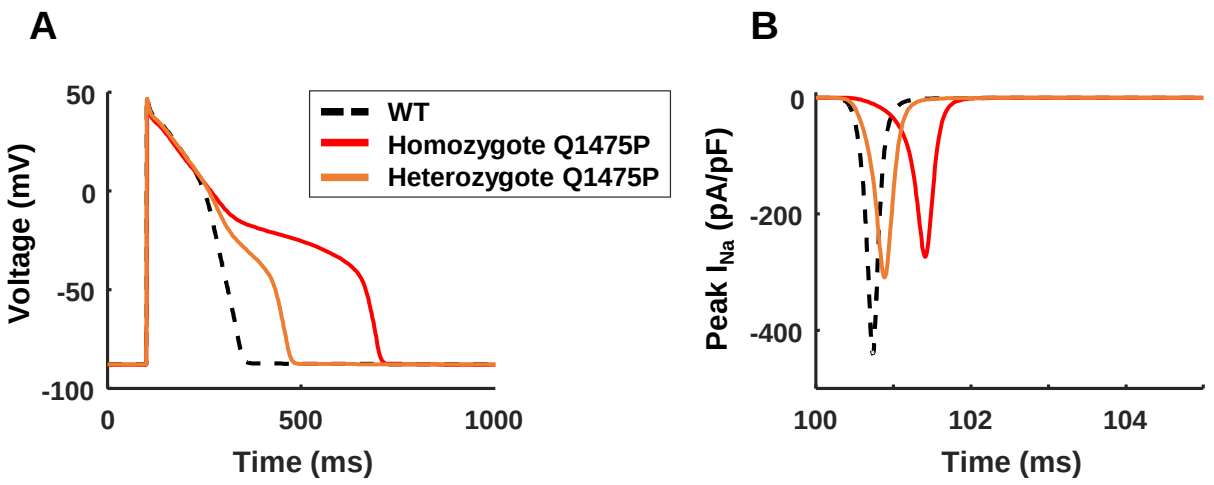

Figure S2: Heterozygous cells show an intermediate phenotype. When incorporated into a model of the ventricular cardiac myocyte, heterozygous Q1475P channels lead to (A) an intermediate action potential duration which is shorter than that of homozygous Q1475P cells and longer than that of WT cells and (B) an intermediate peak sodium current which is larger than that of homozygous Q1475P cells and smaller than that of WT cells.

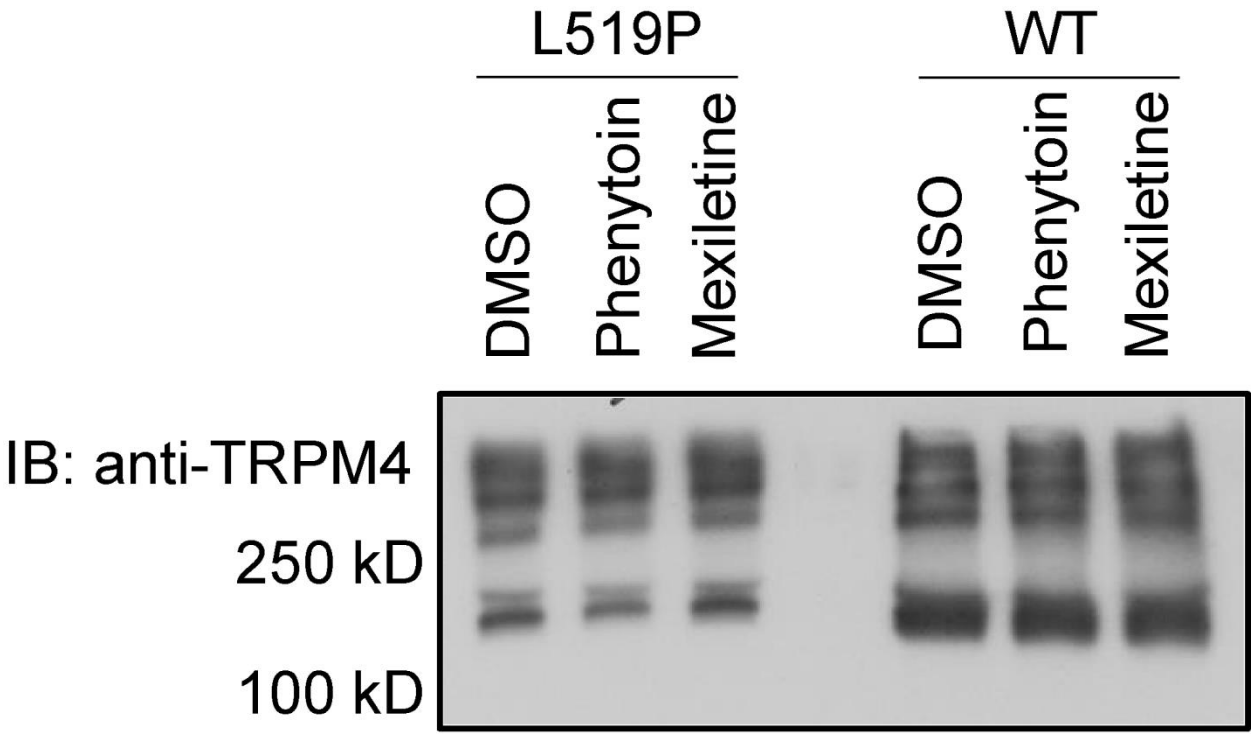

Figure S3: **Phenytoin does not rescue the defective surface trafficking of TRPM4-L519P**. HEK293 cells transfected with WT, or L519P TRPM4 were preincubated for 48h with 100 µM mexiletine, 100 µM phenytoin or with only solvent as a control (DMSO). Western blotting was performed with cell lysates (left) or with the surface biotinylated protein fractions (right).

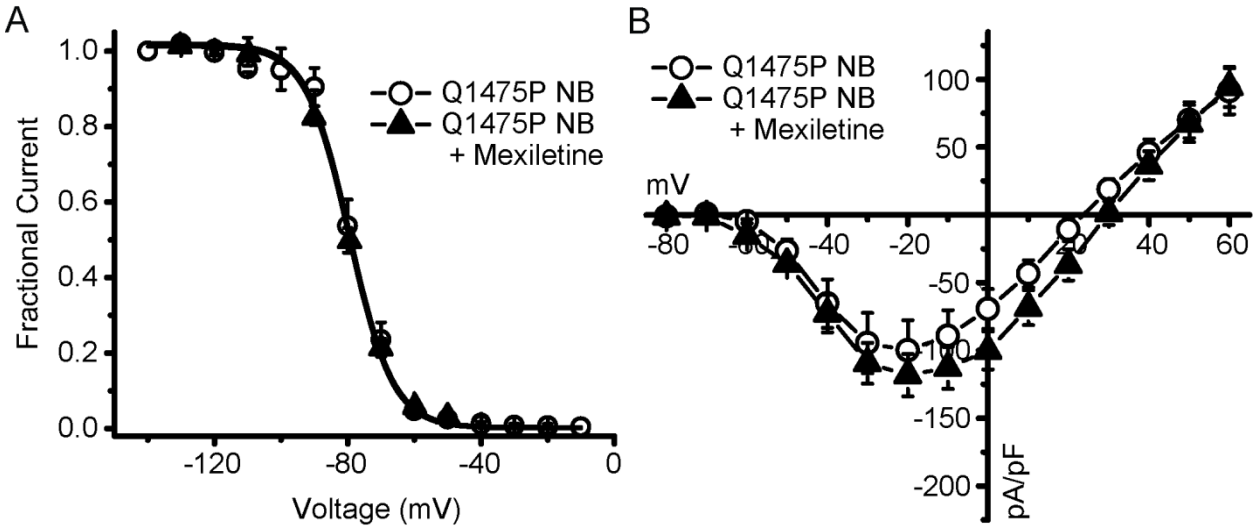

Figure S4: Verification that the F1760A and F7167A mutations disrupt mexiletine binding. HEK293 cells were transfected with Nav1.5(Q1475P)NB, bearing mutations F1760A and F7167A designed to disrupt mexiletine binding. Experiments were performed with cells with or without preincubation with 100 μM mexiletine for 48 h. Shown are (A) steady-state inactivation curves and (B) whole-cell current-voltage relationships.

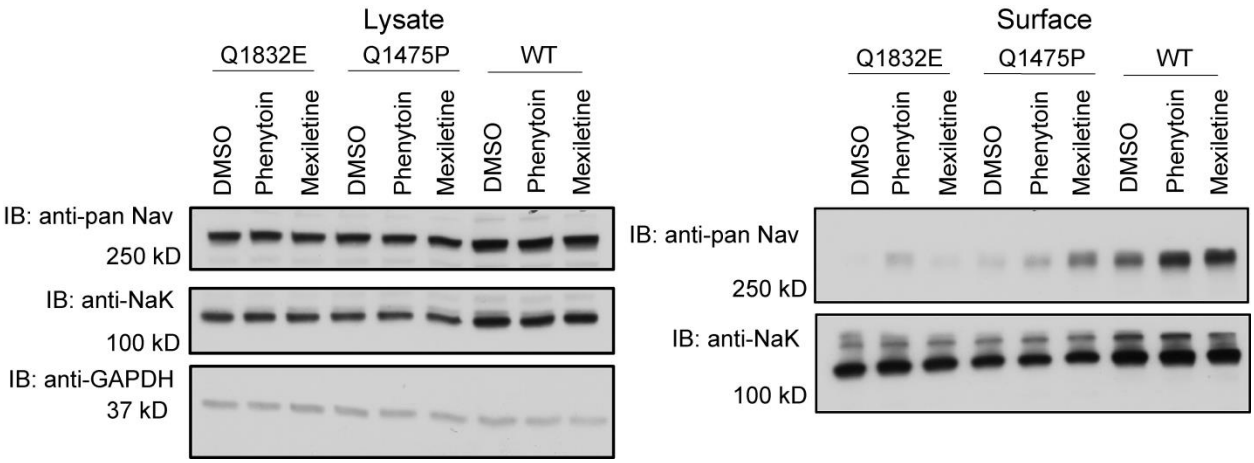

Figure S5: **Phenytoin rescues the defective surface trafficking of $Na_v1.5$-Q1832E**. HEK293 cells transfected with WT, Q1475P or Q1832E $Na_v1.5$ were preincubated for 48h with 100 µM mexiletine, 100 µM phenytoin or with only solvent as a control (DMSO). Western blotting was performed with cell lysates (left) or with the surface biotinylated protein fractions (right). Na^+/K^+ ATPase and GAPDH were used as loading controls. The blot shown is representative blot of two similar experiments.

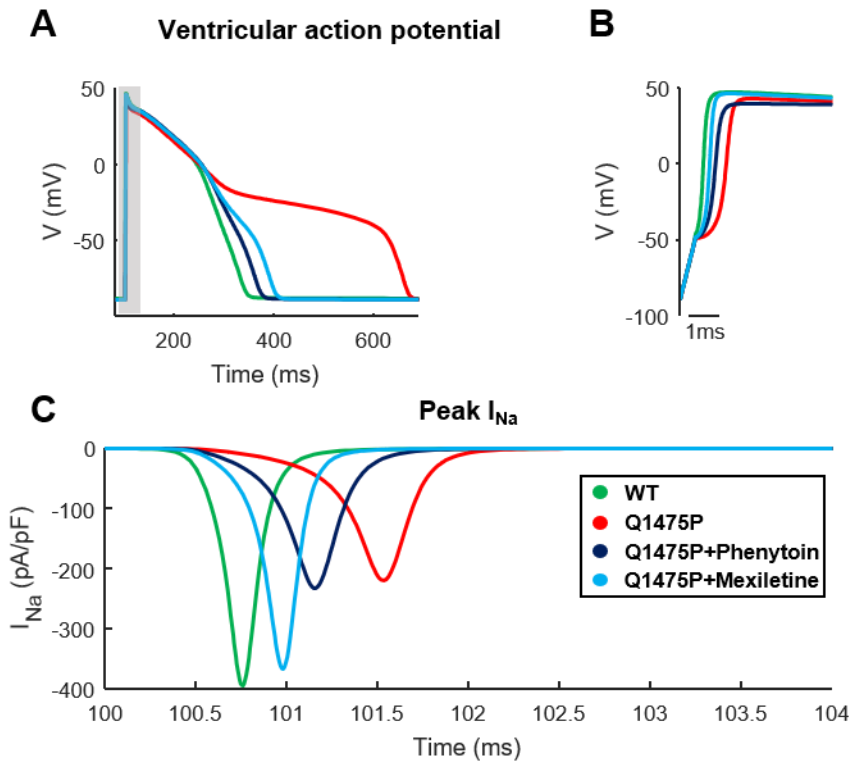

Figure S6: Simulation of human ventricular action potentials incorporating the $Na_v1.5$ rate constants obtained through parameter optimization. (A) Simulations of a ventricular myocyte model predict that Q1475P Na^+ channels (red) produce longer action potentials than WT (green) or Q1475P channels treated with either phenytoin (dark blue) or mexiletine (light blue). For each type of channel, the action potential generated by the median genetic algorithm solution is shown. (B) The upstroke phase of the action potential highlighted in the grey box in panel A. It shows smaller peak action potential and slower upstroke velocity in Q1475P cells and phenytoin treated cells compared to WT and mexiletine treated cells. (C) Analysis of peak Na^+ current during action potential simulations. Panels A and C are adapted from Figure 8A and 8C of the manuscript.

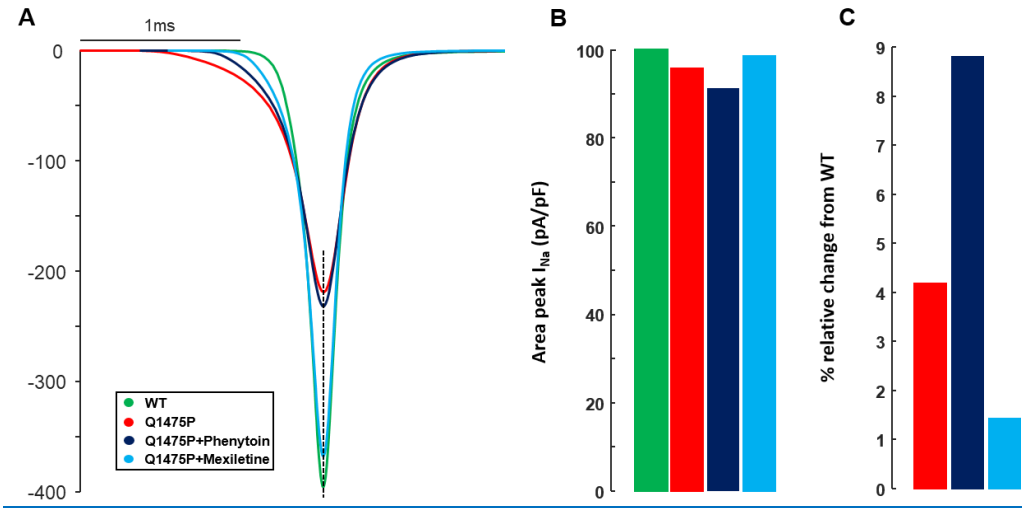

Figure S7: Analysis of peak I_{Na}: amplitude and total area. (A) Traces for peak I_{Na} are shifted in time so that for each cell the peak occurs at the same time point. (B) The area under the I_{Na} curve shown in A is computed and quantified for each cell type. (C) The changes in area relative to WT are shown. Q1475P cells have a 4% decrease in total area compared to WT, while cells treated with phenytoin and mexiletine show a 9% and a ~1% decrease, respectively.